Research Square

Preprints are preliminary reports that have not undergone peer review.
They should not be considered conclusive, used to inform clinical practice,
or referenced by the media as validated information.

The southward movement preference of large-scale persistent extreme precipitation events over the Yangtze River Valley during Mei-yu period

Jiao Ma (15611531586@163.com)
IAP CAS: Institute of Atmospheric Physics Chinese Academy of Sciences https://orcid.org/0000-0001-6456-222X

Ke Wei
IAP CAS: Institute of Atmospheric Physics Chinese Academy of Sciences

Wen Chen
IAP CAS: Institute of Atmospheric Physics Chinese Academy of Sciences

Research Article

Keywords: extreme rainfall events, Mei-yu rainfall, latent heating, potential vorticity, East Asian summer monsoon

Posted Date: February 23rd, 2022

DOI: https://doi.org/10.21203/rs.3.rs-1330055/v1

License: This work is licensed under a Creative Commons Attribution 4.0 International License.
Read Full License

Abstract

Among all rainfall events, heavy rainfall that affects large areas and persists for days can cause serious flooding, severe casualties, and substantial economic losses. In this study, we identify the extreme precipitation events that affect a large area and have persistence of more than three days (LPEPEs) in China during 1961-2013. Most LPEPEs prefer to occur in summer and over southern China, coinciding well with the rainy season in China. The movement of LPEPEs is dominated by the tendency to extend southward, especially for the LPEPEs during the Mei-yu period. The dynamical composite analysis shows that the southward extension is generated by the combined effect of circulation configuration and the diabatic heating caused by large-scale condensation. The mid-level latent heating is associated with a cyclonic anomaly and potential vorticity (PV) maximum. Therefore, westerly and easterly anomalies are produced to the south and north of the heating center, respectively. This kind of circulation anomaly configuration helps create a pattern with positive and negative PV tendency to the south and north of the heating center, leading to LPEPE system development to the south of the precipitation center. Therefore, the LPEPE rainband has a preference to move southward over the Yangtze River Valley during the Mei-yu period. We also test the dynamical mechanism with a numerical sensitivity experiment using the WRF model. In the experiment without latent heating feedback, the Mei-yu rainband moves northward and extends to central and North China. While in the experiment with the latent heating feedback, the rainband intensifies and extends southward. The southward extension preferences of the LPEPE can provide an internal dynamical of the stagnation of East Asian summer evolution.

1. Introduction

The large-scale persistent extreme precipitation events (LPEPEs) are the most dangerous, usually causing catastrophic flooding, severe casualties, and tremendous economic losses over a vast region. They have been the focus of disaster monitoring, prevention, and mitigation for research agencies and governments at all levels. In addition to severe floods over a vast region, LPEPEs can also cause secondary debris flows, soil erosion, landslides, epidemics, crop failure, urban and rural waterlogging. For the densely populated East Asia, the most vulnerable regions to LPEPEs are the Yangtze River Valley, Huaihe River Valley, and South China (Bao, 2007; Tang *et al.*, 2006), especially during the Mei-yu period, usually from mid-June to mid-July when the monsoon rain belt dominates the precipitation over East Asia.

The LPEPEs are closely related to the Mei-yu rain belt, East Asian summer monsoon, and tropical cyclones (Luo *et al.*, 2016; Wu *et al.*, 2019). While the frequency of precipitation events decreased by 10% from 1960 to 2000 for eastern China (Liu *et al.*, 2005), the frequency and intensity of LPEPEs show an increasing trend from 1960 to 2013 (Wu *et al.*, 2019). Zhao *et al.* (2010) found that the persistent rainfall in the 1980s-1990s began earlier and ended later over southern China, lengthening the rainy season by 23 days compared with the 1960s-1970s. Studies have focused on the location, time variation, mesoscale systems, and the synoptical characteristics of different LPEPEs (Bao, 2007; Luo *et al.*, 2016; Wu *et al.*, 2019). Relatively, much less effort has been devoted to understanding the movement and associated internal dynamics of LPEPEs.

Some LPEPEs move a long distance from where they are originally identified, covering a large area. For example, the LPEPE that occurred from June 30th to July 2nd, 1995 (Du *et al.*, 1996) due to a low-level vortex moving eastward from east of the Tibetan Plateau to the lower reaches of the Yangtze River in southern China, causing a large-scale flood to Dongting Lake, Xiang River, Zishui River, and Yuan River (Wang, 1995). Some LPEPEs remain almost stagnant during the rainfall period. For example, the LPEPE from July 8th to July 10th, 2003, was caused by the shear lines in Mei-yu front and two mesoscale vortexes over the shear region. It brought persistent heavy rainfall there, resulting in the second-highest water level of Hongze Lake since 1949 and the worst flooding since the 1991 flood (Zhao *et al.*, 2010).

In this study, we focus on the mobility and internal dynamics of large-scale persistent extreme precipitation events in China, with attention to the direction preference of LPEPE. Since LPEPEs can cause serious consequences, whether the LPEPE stays in one region or moves far away will be crucial for successful disaster prevention. Using high-resolution precipitation data, we identified the LPEPEs from 1961 to 2013 and found a southward extension preference of LPEPEs during the Mei-yu period. In section 3 and section 4, we discussed the dynamical mechanism of the mobility of LPEPE and pointed out that the latent heating of the LPEPEs has a self-maintaining effect that can reinforce the rainfall system and cause the system to have a southward extension preference. The discussion of the results and conclusion are provided in section 5.

2. Data And Methodology

2.1. Data

The daily and monthly precipitation grid data set (V2.0) is derived from China's high-density ground stations (2472 national meteorological observation stations) by the National Meteorological Information Center of China Meteorological Administration (CMA) (http://data.cma.cn). This grid dataset has a horizontal resolution of 0.5°×0.5° from 1961 to 2013, and the spatial interpolation is based on the TPS (thin-plate spline) method. It can accurately reflect the spatial and temporal variation characteristics of precipitation (Zhao *et al.*, 2014). This dataset has been widely used in precipitation-related studies (Zhang *et al.*, 2017; Zhao *et al.*, 2019).

In addition, the circulation parameters of wind, geopotential height, and temperature are adopted from the fifth-generation ECMWF reanalysis (ERA5), which has a horizontal resolution of 0.25° ×0.25° and 37 vertical levels from 1000 hPa to 1 hPa. The ERA5 dataset is used to analyze the synoptic characters, calculate the atmospheric apparent heat source (Q_1), the apparent moisture sink (Q_2), and the potential vorticity tendency equation, and initialize the numerical simulation experiment. The onset and retreat dates of the Mei-yu period in China are based on the “Indices of mei-yu Monitoring” (Shao, 2016). According to this criteria, Mei-yu includes three types in China: Mei-yu □ in the south of the Yangtze River, Mei-yu □ in the middle and lower reaches of the Yangtze River, and Mei-yu □ in the Yangtze-Huaihe River basin. In this study, the Mei-yu period includes all three types.

2.2. Methodology

2.2.1. Definition of LPEPE

Several methods were used to define the large-scale persistent extreme precipitation events (Bao, 2007; Chen and Zhai, 2013; Ren *et al*., 2012). Since we focus on the mobility feature of LPEPEs, the objective identification technique for extreme regional events ("candied fruits" method) (Ren *et al*., 2012) is utilized in this study. The LPEPE is detected in the following steps and criteria (concept diagram illustrating in Fig. 1a). Firstly, the large-scale extreme precipitation patterns (LEPs) are identified as the sizeable continuous region (the grid number no less than 60 for the 0.5×0.5 latitude-longitude grid dataset, approximately 14×10^4 km^2) with the daily precipitation no less than 25 mm at each grid (Bao, 2007; Chen and Zhai, 2012; Ren *et al*., 2012). Secondly, a large-scale persistent extreme precipitation event (LPEPE) is defined as an LEP persisting for at least three days. The LEPs of two consecutive days are considered the same event when the LEP coincidence degree is greater than 20% (Wang *et al*., 2014). Finally, the LPEPE are screened to keep the extreme events that the maximum total precipitation is no less than 250 mm. During 1961-2013, 82 LPEPEs were identified, with the date and duration information listed in Table 1.

Table 1

Detailed information on all LPEPEs. “Day 1” is the first day of an LPEPE, and “**Duration”** is the time span of an LPEPE. “WP1” is averaged latitude and longitude of all grids in the LEP weighted by the daily precipitation on the first day of the LPEPE. The bold font LPEPEs are caused by typhoons. The asterisk LPEPEs occur during the Mei-yu periods.

Day1	Duration	WP1	Day1	Duration	WP1
*19610531	3	(27.28, 115.34)	19920324	5	(28.08, 115.39)
*19610609	4	(28.10, 113.5)	*19920703	4	(28.59, 114.96)
19620724	**3**	**(38.99, 116.05)**	*19930703	3	(28.94, 115.12)
*19630709	3	(32.81, 115.11)	*19940612	6	(27.80, 112.5)
19630807	3	(39.04, 114.34)	*19950615	3	(27.05, 114.94)
19640612	4	(24.94, 116.55)	*19950620	7	(31.51, 114.32)
*19640624	3	(29.32, 113.32)	*19950630	3	(27.14, 110.26)
*19660701	3	(23.13, 110.67)	19950724	3	(33.01, 109.72)
19670804	**4**	**(23.41, 110.39)**	**19951003**	**3**	**(23.15, 112.03)**
19680617	3	(25.73, 111.9)	*19960702	3	(30.20, 116.13)
*19680713	4	(31.78, 114.2)	*19960714	4	(30.06, 112.86)
*19690623	4	(29.34, 112.62)	**19960801**	**3**	**(26.09, 118.14)**
*19690715	3	(30.87, 117.36)	*19970707	5	(28.12, 113.28)
*19700625	5	(28.60, 116.47)	**19970819**	**3**	**(32.64, 119.06)**
*19700710	5	(27.29, 115.17)	*19980618	4	(28.98, 116.39)
*19710609	3	(33.51, 112.82)	*19980623	4	(25.26, 114.58)
19730526	3	(24.18, 108.93)	*19980721	3	(29.66, 110.62)
*19730623	3	(29.15, 115.07)	19990415	3	(29.27, 115.11)
19730905	3	(31.94, 108.12)	19990524	3	(26.29, 115.95)
19750729	3	(38.90, 115.03)	*19990626	4	(29.60, 112.34)
19750813	**3**	**(28.45, 117.59)**	*20000609	3	(27.16, 115.81)
*19760707	3	(24.50, 110.04)	20010531	3	(24.65, 100.25)
*19800731	3	(29.47, 112.78)	**20010706**	**3**	**(23.96, 114.07)**
*19810627	5	(29.41, 111.25)	*20020614	4	(27.08, 115.03)
*19820614	4	(27.94, 112.15)	20020722	4	(29.63, 113.25)

Day1	Duration	WP1	Day1	Duration	WP1
*19820619	3	(29.04, 114.08)	**20020806**	**3**	**(24.42, 114.59)**
19820727	3	(30.94, 107.19)	*20030624	3	(28.90, 116.35)
19820730	4	(35.78, 110.75)	*20030708	3	(29.99, 111.6)
19820817	**3**	**(24.15, 113.1)**	*20040718	3	(28.30, 110.65)
19830731	3	(25.37, 102.58)	20050618	6	(27.69, 115.87)
19831004	4	(33.23, 111.04)	*20060606	3	(27.12, 114.75)
*19840612	3	(32.21, 112.22)	**20060714**	**4**	**(26.41, 118.41)**
19840831	**3**	**(25.76, 115.28)**	20070607	4	(24.73, 112.09)
*19860621	3	(28.58, 111.38)	*20070617	3	(33.66, 106.5)
*19870702	3	(28.80, 113.12)	20070819	4	(26.24, 118.41)
19880507	3	(29.75, 114.34)	20080828	3	(30.82, 110.06)
19880922	**3**	**(26.08, 117.69)**	20081031	3	(24.70, 107.53)
*19890616	3	(30.22, 116.11)	*20090701	4	(28.18, 117.58)
*19890629	5	(27.41, 111.85)	*20100618	3	(26.64, 116.39)
*19900618	3	(33.98, 112.45)	**20110930**	**3**	**(23.31, 108.66)**
19910906	**3**	**(27.08, 118.59)**	*20120622	3	(25.60, 114.83)

2.2.2. The location of LEP

The average location of all grids in the LEP weighted by the daily precipitation, WP (Lat_{wp}, Lon_{wp}), is used as the location of LEP. Meanwhile, two other methods are adopted to verify the location of an LEP. 1) MP (Lat_{mp}, Lon_{mp}), the location of the maximum precipitation grid. 2) AP (Lat_{wp}, Lon_{wp}), the average latitude of maximum precipitation for each longitude in the LEP (Lat_{ap}), and the average longitude of maximum precipitation for each latitude (Lon_{ap}) in the LEP.

The direction of an LPEPE is considered as the vector from the LEP location of the first day to the last day. If the latitude difference of an LPEPE between the last day and the first day is negative, the event is then classified as a southward extension LPEPE. Accordingly, three vectors can be defined using MP, WP, and AP. An example is shown in Fig. 1b, which is the MP, WP, and AP of an LPEPE randomly chosen on Jun 21st, 1986. The LPEPE is mainly caused by the southwest vortex over the middle reach of Yangtze River; the maximum daily precipitation is 263 mm, breaking the historical records in the Huangshi City (Ge *et al.*, 1989).

2.2.3. Apparent heat source and apparent moisture sink

The apparent heat source (Q_1) and apparent moisture sink (Q_2) are analyzed to investigate the thermal dynamical characters and moisture characters of LPEPEs. The function of Q_1 and Q_2 are described in (Hsu and Li, 2011). Here Q_1 represents the total diabatic heating (including radiation, latent heating, and surface heat flux). Q_2 represents the latent heating due to condensation or evaporation processes and subgrid-scale moisture flux convergences (Yanai *et al.*, 1973).

$$\langle Q_1 \rangle = \frac{1}{g}\int_{p}^{p_s} Q_1 dp$$

1

,

$$\langle Q_2 \rangle = \frac{1}{g}\int_{p}^{p_s} Q_2 dp$$

2

,

2.2.4. Potential vorticity (PV) tendency equation

To investigate the internal dynamical processes of the LPEPEs during the Mei-yu period, the Ertel potential vorticity (PV) equation is diagnosed. The PV in pressure coordinates is

$$\mathrm{PE} = -\mathrm{g}(\mathrm{f}+\xi)\frac{\partial \theta}{\partial \mathrm{p}} + \mathrm{g}\left(\frac{\partial \mathrm{v}}{\partial \mathrm{p}}\frac{\partial \theta}{\partial \mathrm{x}} - \frac{\partial \mathrm{u}}{\partial \mathrm{p}}\frac{\partial \theta}{\partial \mathrm{y}}\right)$$

5

,

in which f is the Coriolis parameter, θ denotes the potential temperature, u and v represent zonal and meridional winds, respectively. PE is the Ertel PV. After removing the small terms and coordinate transformations (Li *et al.*, 2011; Li *et al.*, 2019), the PV tendency equation without frictional effects can be written as

$$\frac{\partial \mathrm{PE}}{\partial \mathrm{t}} = -\frac{\partial \mathrm{uPE}}{\partial \mathrm{x}} - \frac{\partial \mathrm{vPE}}{\partial \mathrm{y}} - \frac{\partial \omega \mathrm{PE}}{\partial \mathrm{p}} + \mathrm{g}\frac{\partial \mathrm{v}}{\partial \mathrm{p}}\frac{\partial \mathrm{Q}}{\partial \mathrm{x}} - \mathrm{g}\frac{\partial \mathrm{u}}{\partial \mathrm{p}}\frac{\partial \mathrm{Q}}{\partial \mathrm{y}} - \mathrm{g}(\mathrm{f}+\xi)\frac{\partial \mathrm{Q}}{\partial \mathrm{p}}$$

6

,

Where $\xi = \frac{\partial \mathrm{u}}{\partial \mathrm{x}} - \frac{\partial \mathrm{v}}{\partial \mathrm{y}}$ is the vertical vorticity. Q is the diabatic heating, there Q_1 is used as Q. $-\frac{\partial \mathrm{uPE}}{\partial \mathrm{x}} - \frac{\partial \mathrm{vPE}}{\partial \mathrm{y}}$ (*PE1*+*PE2*) is the horizontal PV flux divergence, and $-\frac{\partial \mathrm{wPE}}{\partial \mathrm{p}}$ (*PE3*) is the vertical PV flux divergence. $-\mathrm{g}\frac{\partial \mathrm{u}}{\partial \mathrm{p}}\frac{\partial \mathrm{Q}}{\partial \mathrm{y}}$ (*PE4*) and $\mathrm{g}\frac{\partial \mathrm{v}}{\partial \mathrm{p}}\frac{\partial \mathrm{Q}}{\partial \mathrm{x}}$ (*PE5*) are the redistribution of PV induced by the uneven distribution of Q in

meridional and zonal directions, while the last term is induced by the vertically uneven distribution of *Q* (*PE6*).

2.2.5. Composite method

Considering the moving features of LPEPEs, both the traditional and dynamic composite methods are used. In the dynamic composite, the location of LEP (here WPs are used) is taken as the origin of coordinates, then to make a composite for every LPEPE in the same scope on each day in the moving coordinate system. Thus, the composite center is the origin of the coordinates, which moves along with the LPEPE, and the coordinates indicate the distances to the composite center (Li *et al.*, 2019). Since the majority of LPEPEs persist for three days (54 out 82 LPEPEs, 67%), we use the first three days' dynamic composite analysis results. Three degrees departing from the composite center in meridional direction and zonal direction can well reflect the adjacent dynamic and thermal dynamic features. The dynamic composite analysis method also has been used in studies on southwest vortices and typhoons (Li *et al.*, 2014; Li *et al.*, 2004).

2.2.6. Model setup and design of sensitivity experiments

The non-hydrostatic version 4.2 of the Weather Research and Forecasting Model (WRF) (Skamarock *et al.*, 2019) was adopted to simulate the LPEPE and analyze its characteristics and evolution. The model has 38 sigma levels in the vertical and the model top is set to 50hPa. the main model schemes include (i) the Kain-Fritsch (new Eta) cumulus parameterization scheme (Kain, 2004), (ii) the Kain-Fritsch (new Eta) cumulus parameterization scheme (Kain, 2004), (iii) the Goddard scheme (Tao *et al.*, 1989; Tao *et al.*, 2016) for microphysics, (iv) the YSU scheme (Fairall *et al.*, 2003) for the boundary layer, (v) the Noah Land Surface scheme (Alapaty *et al.*, 2008) for the land surface layer, (vi) the RRTM scheme for longwave (Mlawer *et al.*, 1997), (vii) and the Dudhia's scheme (Dudhia, 1989) for shortwave radiation parameterization.

Considering the influence of latent condensation heat and internal thermodynamics, the effects of latent heating on the mobility of LPEPE were investigated through sensitivity experiments. The latent heat release associated with cloud microphysics and the cumulus parameterization scheme was turned off in the sensitivity run (SEST); therefore, the latent head has no feedback on the circulation. In the control run (CTRL), however, the model is run with full physics, so the latent heat has forcing on the circulation. The model simulation was carried out for a randomly chosen LPEPE in 2003. The WRF model was run 119 hours starting at 0000 UTC 7th July, 2003, using the ERA5 dataset at intervals of six hours as the initialization. Fig. 2 shows the domain used for all simulations, covering eastern China and the South China Sea, with a horizontal resolution of 5 km. All the experiments are launched with identical initial and boundary conditions.

3. The Spatial And Temporal Distribution

In this study, we detected 82 LPEPEs (Table 1) from 1961 to 2013. According to the Report of the Damage Caused by Disaster in China from 1949 to 1995 (Zhang and Fan, 1995) and the disaster conditions and

disaster reports published annually in the Journal “Disaster Reduction in China”, there is a close relationship between the flooding disasters and the LPEPEs, with 69 out of 82 LPEPEs (more than 84%) associated with flooding disasters. For the rest 13 LPEPEs, ten of them occurred in the period from 1966 to 1976, when the disaster datasets were often lost.

The number of LPEPEs during the 1990s and 2000s is more than in other decades, with 22 LPEPEs occurring in the 1990s, 18 in the 2000s, 9 in the 1970s and 17 in the 1980s. Zou and Ren (2015) pointed out that China experienced more severe and extreme regional rainfall events in the 1990s. The years with more than two LPEPEs are 1973, 1982, 1995, 1996, 1998, 1999, 2002, and 2007. Most LPEPEs occurred in the summer season, with 32 in June, 26 in July and 10 in August (Fig. 3a). According to the dataset of landfall tropical cyclones by (Ying *et al.*, 2014), 15 LPEPEs are related to typhoons. As we mainly focus on the characteristics of LPEPEs in the Yangtze River Valley during Mei-yu, which is considered the results of the mid-latitude front system, we exclude the typhoon-associated cases, resulting in 67 LPEPEs. Among them, 46 LPEPEs occurred in the Mei-yu period (LPEPEs-M). The LPEPEs-M (asterisk) and typhoon-associated LPEPEs (bolded) are listed in Table 1.

Most LPEPEs prefer southern China and eastern China, with 94% and 98% occurring south of 35°N, and east of 105°E, respectively (Fig. 3d). Using the distribution of MPs (Fig. 3e) and APs (Fig. 3f) got similar results (Figures not shown). The temporal and spatial distribution of LPEPEs is similar to the previous studies (Bao, 2007; Chen and Zhai, 2012; Tang *et al.*, 2006).

The LPEPE direction, defined as the displacement vector difference of MPs (or WPs and APs) between the last day and the first day of the LPEPE, has a preference to shift southward (Fig. 3b), especially for LPEPEs-M (Fig. 3c). Using WPs, 33 out of 46 (72%) LPEPEs-M move southward. The ratio is similarly high if MPs or APs are used, which is 31 out of 46 (67%) for MPs, and 32 out of 46 (70%) for APs (Fig. 3c).

Why do the LPEPEs prefer southward movement, and what is the mechanism of the southward-moving LPEPEs. Considering the more significant southward movements feature of LPEPEs-M and a relative coincident background condition during the Mei-yu period, the southward-moving LPEPEs-M (33 cases detected using WPs) are analyzed in the following sections. Using APs or MPs show similar dynamical features as the WPs (results not shown).

4. The Dynamical And Thermodynamical Features Of Southward-moving Lpepes-m

The composite of the 33 southward-moving LPEPEs-M reveals the typical circulation configuration during the LPEPEs over the Yangtze River valley (Fig. 4), which usually include the following key components:

1. the eastward extension of the high-level South Asian High (SAH), represented by the 1252-dagpm contour lines at 200 hPa.
2. the persistence of Western Pacific Subtropical High (WPSH), represented by the 588-dagpm contour lines at 500 hPa.

3. the combination of low-level convergence (dashed lines in Fig. 4d-4f) and high-level divergence (black contour lines in Fig. 4a-4c)
4. the low-level southwesterly (shadings in Fig. 4d-4f) and high-level westerly (shadings in Fig. 4a-4c).

During the rainfall process, the high-level divergence center shifts southwestward from the Yangtze River to South China (Fig. 4a, Fig. 4c). The high-level jet weakens, and the low-level jet over South China gets weaker and retreats southward. Usually, the low-level jet is associated with a large amount of warm and moist air. Thus, the abundant moisture supplement also retreats southward. The low-level convergence core locates to the north of the jet and the northwest of WPSH, gets weaker and retreats southward (Fig. 4d-4f). And the WPSH retreat eastward from 119°E to 126°E. As a joint result of high-level divergence and low-level convergence, there is a favorable dynamical condition for a strong and southward-moving upward motion over the Yangtze River (Du *et al.*, 2008).

During LPEPEs, latent condensation heating is the major contributor to diabatic heating (Fig. 4g – Fig. 4i). Q_1 shows similar characteristics as Q_2, both moving southward from the lower reach of the Yangtze River to South China (Fig. 4g – Fig. 4i), indicating that the atmospheric heating sources from the latent condensation heating of the intense precipitation. Liu (1999) points out the latent condensation heat of the Mei-yu rainband will force a cyclone anomaly below the center of diabatic heating (below 400hPa-500hPa) within a short time by depressing the isobaric surface. Since the rainband is over the northwest of WPSH, the cyclone anomaly forced by the diabatic heating is also located along the northwest of WPSH. As a result, it obstructs the northward migration of the WPSH and the Meiyu rain belt.

The low-level convergence and high-level divergence are favorable for the ascending motion, which is shown in Fig. 5 for the dynamic composites on the height-meridional cross-sections. The strong upward motion is verified above the Lat_{wp}, associated with convergence at the lower levels and divergence at higher levels. With the Lat_{wp} shifting southward, from the black dot to the red dot, the upward motion center also moves southward (Fig. 5a – Fig. 5c), which pushes the rainband southward.

5. The Pv Tendency Diagnosis

The dynamic composite analysis of PV tendency equation is calculated to determine the mechanism of diabatic latent heat manipulating the meridional movement of LPEPEs-M. The dynamic composite analysis of the PV tendency equation (Li *et al.*, 2019) at 850hPa was calculated (Fig. 6). The positive values of "*PE1*" to "*PE6*" increase the *PE*, helping enhance the cyclone or weaken the anticyclone, and therefore contribute to the precipitation of the rainband and the related condensation latent heat. Contrarily, the negative values weaken the cyclone and contribute to the decay of the rainfall system. "*PE1*+*PE2*" is the horizontal PV flux divergence, as shown in Fig. 6a to Fig. 6f. They are usually the opposite, with *PE1* decreasing the system and *PE1* increasing the system, respectively. The vertical PV flux divergence (*PE3*) weakens the PV along and south of the rainband. Generally, the uneven distribution of PV influences the precipitation intensity along the rainband of these southward-moving LPEPEs-M.

As for thermodynamical factors, the redistribution of PV, which arises from the uneven distribution of Q in the meridional direction, is the dominating factor in the meridional movement of the LPEPEs-M. Fig. 6j to Fig. 6l shows a dipole pattern of *PE4*, with positive in the south and negative in the north. As the Mei-yu rainband has a zonal orientation, this causes $\frac{\partial Q}{\partial y}>0$ to the south of the rainband and $\frac{\partial Q}{\partial y}<0$ to the north, The dipole pattern of *PE4* is mainly associated with the vertical distribution of zonal wind. Around 600hPa, there is a westerly anomaly center over south of the rainband (Fig. 5d-Fig. 5f), caused by the cyclone anomaly, which is related to the diabatic heating of the rainband (Liu, 1999). Therefore, even though there is a low-level jet with its core around 850hPa (Joseph and Sijikumar, 2004) to the south of the rainband, the wind pattern makes $\frac{\partial u}{\partial p}<0$ below 600hPa in this region, resulting in a positive effect on PV tendency at the lower levels to the south of the rainband. To the north of the rainband, the cyclone anomaly generates an easterly anomaly (Liu, 1999). As a result, the westerly is relatively weaker than to the south of the rainband at the same level below the diabatic heat core (around 500hPa).

Coupling with the meridional distribution of Q, the vertical distribution of westerly is favorable for the southward extension of the rainband of LPEPEs-M, or prevent the rainband from moving northward. Compared with other terms, the uneven distribution of Q in zonal direction (*PE5*) is the weakest. The vertical gradient of Q (*PE6*) is positive over the rainband and to its south, which helps to strengthen the precipitation intensity of the rainband and favors the southward movement of the rainband slightly.

In conclusion, the persistence of the PV is mainly maintained by the horizontal PV flux divergence in the meridional direction (*PE2*), and the vertically uneven distribution of Q (*PE6*). While the southward extension is mainly caused by the redistribution of PV (*PE4*), which arises from the uneven distribution of Q in the meridional direction, and is partially contributed by *PE6*

6. The Simulation Of 2003 Lpepe

To investigate the effect of latent heat in the mobility of LPEPEs, sensitivity numerical experiments were carried out for a randomly chosen southward extension LPEPE from July 8th to July 10th, 2003. The model description and experiments design are introduced in section 2.2.6.

The rainband of this event slightly shifts southward over the north of the Yangtze River (Fig. 7a – Fig. 7c, shades), and the rainfall is mainly caused by two low vortexes along the shear line (Zhou and Li, 2010). Meanwhile, the west ridge of WPSH (represented with 150dagpm at 850hPa) extends around Taiwan Strait (Fig. 7a – Fig. 7c, contour) and shows eastward retreat.

The CTRL run simulates a similar stagnant rainband and a slightly southeastward retreating WPSH (150dagpm, 850hPa) (Fig. 7d – Fig. 7f). While in the sensitivity experiment, which turns off the latent heating effect, the persistence of the rainband is not reproduced. The simulated rainband migrates from the north of Yangtze River to Huang-Huai Plain (Fig. 7g – Fig. 7i). And the west ridge of WPSH extends more westward and norward in the sensitivity experiment than the observation and CTRL run. Therefore, without the latent heat forcing, the rainband and WPSH migrate northward significantly. And the latent

heating is the critical intrinsic forcing that leads to LPEPEs persistence of rainfall belt over the Yangze River Valley.

The geopotential height difference between the CTRL and SEST shows a cyclone anomaly over the Mei-yu rainband (Fig. 8a – Fig. 8c), which can be explained by Liu (1999) that the condensation latent heating forces a cyclone anomaly below the heating center (about 400hPa-500hPa) by depressing the isobaric surface. The cyclone anomaly moves northeastward from Southwest China to the middle and lower reaches of the Yangtze River (around 115°E), obstructing the WPSH's northward migration.

The zonal wind difference shows a westerly anomaly to the south of the rainband, and an easterly anomaly to the north of the rainband at the low level (Fig. 8a-Fig. 8c). The condensation latent heat difference extends from the low level to the middle level, and the center is over the middle level (about 500hPa) (Fig. 8d-Fig. 8f, Fig. 8g-Fig. 8i), therefore, leading to $\frac{\partial Q}{\partial y}$>0 and $\frac{\partial u}{\partial p}$<0 below 600hPa to the south of the rainband; $\frac{\partial Q}{\partial y}$<0 and $\frac{\partial u}{\partial p}$<0 to the north of the rainband. This will lead to positive *PE4* and negative *PE4* to the south and north of the rainband, respectively, leading to system development to the south. So that, the condensation latent heat obstructs the rainband from migrating northward, favors the rainband shifting southward. Analysis of the vertical cross-section along another longitude (e.g., 114°E) show similar processes (figures not shown).

7. Conclusion And Discussion

We defined the LPEPE as a large continuous region (the grid number no less than 60 for the 0.5×0.5 latitude-longitude grid dataset) with the daily precipitation no less than 25mm that can persist (the overlap rate no less than 20%) for at least three days, and the total maximum daily precipitation is more than 250mm. Using this definition, 82 LPEPEs were detected from 1961 to 2013, among which 15 LPEPEs were related to typhoons. After excluding the typhoon-related LPEPEs, we got 46 LPEPEs in the Meiyu period.

We found that the LPEPEs have the tendency to move southward, especially during the Mei-yu period 2/3 of the LPEPEs tend to shift southward. For southward-moving LPEPEs-M, there is a favorable dynamical condition for strong upward motion above the rainband, introduced by the combined effect of high-level and low-level jets. During an LPEPEs-M, a large amount of latent condensation heat is released at middle levels, compressing a cyclone anomaly in the middle to lower levels above the rainband. Accordingly, the vertical distribution of zonal wind below 600hPa is changed to $\frac{\partial u}{\partial p}$>0. Coupling with the meridional diabatic heating distribution, potential vorticity is generated to the south of the rainband and diminished to the north of the rainband, creating a condition that favors the southward movement of the rainband. This also has the effect of hindering the northward mitigation of the rainfall system. The vertical distribution of diabatic heat also helps intensify the precipitation over the rainband of LPEPEs-M. The sensitivity experiment for a randomly chosen LPEPE from 8th to 10th July 2003 verifies the effect of latent heating in shifting rainband southward and obstructing the Mei-yu system's northward movement.

It's well known that the East Asian summer monsoon is characterized by alternative stagnation and rapid northward movement, usually with three stationary periods and two abrupt northward jumps. Especially during the Mei-yu period, the rain belt stagnates over the Yangzte River Valley for about one month. This remarkable stepwise and standing feature has been explained from the viewpoint of seasonal changes in the general circulation in East Asia (Ding and Chan, 2005; Ye *et al.*, 1958), climatological intraseasonal oscillation (Qian *et al.*, 2002), the continuous southward intrusion of cold air and accompanying frontal systems (Wu and Wang, 2001), warm advection in the mid-troposphere from the Tibetan Plateau (Sampe and Xie, 2010). In this study, we illustrated that the large-scale rainfall could reinforce itself and has the tendency to shift southward, which has the effect of hindering the northward migration of the primary rain belt.

The abundant diabatic heating released of the LPEPE rainfall can reach the extent of typhoons. By forcing secondary circulation, the heating can have a significant impact on the large-scale circulation, therefore, be an intrinsic reason for the rain belt stagnation. This study mainly focuses on LPEPEs during Mei-yu season; the interaction between latent heat and large-scale circulation needs to be further studied for the whole summer season. Meanwhile, whether the size and orientation of rainfall patterns have different feedback to the synoptic system is also an important question that needs further investigation.

Declarations

Acknowledgements

This research was supported by the National Natural Science Foundation of China (Grant No. 41961144025) and the Alliance of the International Science Organizations (Grant No. ANSO-CR-KP-2020-01). In this study, the ERA5 data were provided by the ECMWF and are available online at http://apps.ecmwf.int/datasets/data/. The JRA-55 reanalysis data were obtained from JMA and downloaded from https://jra.kishou.go.jp.

References

1. Alapaty K, Niyogi D, Chen F, Pyle P, Chandrasekar A, Seaman N (2008) Development of the flux-adjusting surface data assimilation system for mesoscale models. Journal of Applied Meteorology and Climatology 47(9):2331-2350. http://doi.org/10.1175/2008jamc1831.1
2. Bao M (2007) The Statistical Analysis of the Persistent Heavy Rain in the Last 50 Years over China and Their Backgrounds on the Large Scale Circulation. Chinese Journal of Atmospheric Sciences 31(05):779-792. http://doi.org/10.3878/j.issn.1006-9895.2007.05.03 (in Chinese)
3. Chen Y, Zhai PP. 2012. Analysis of the Characteristics of Persist Rainstorm in China. *strengthening the scientific and technological base and advancing meteorological modernization-The 29th annual meeting of Chinese Meteorological Society*, Shenyang, Liaoning Province, 12.

4. Chen Y, Zhai PM (2013) Persistent Extreme Precipitation Events in China During 1951-2010. Climate Research 57(2):143-155. http://doi.org/10.3354/cr01171
5. Ding YH, Chan JCL (2005) The East Asian summer monsoon: an overview. Meteorology and Atmospheric Physics 89(1-4):117-142. http://doi.org/10.1007/s00703-005-0125-z
6. Du XL, Li DW, Lan W (1996) Analysis of a rainstorm from 30th June to 2nd July 1995. Journal of Guizhou Meteorology 20(01):26-32. http://doi.org/CNKI:SUN:GZQX.0.1996-01-006 (in Chinese)
7. Du Y, Zhang YC, Xie ZQ (2008) Impacts Of Longitude Location Changes Of East Asian Westerly Jet Core On The Precipitation Distribution During Meiyu Period In Middle-Lower Reaches Of Yangtze River Valley. Acta Meteorologica Sinica 66(4):566-576. http://doi.org/10.3321/j.issn:0577-6619.2008.04.010 (in Chinese)
8. Dudhia J (1989) Numerical Study of Convection Observed during the Winter Monsoon Experiment Using a Mesoscale Two-Dimensional Model. Journal of the Atmospheric Sciences 46(20):3077-3107. http://doi.org/10.1175/1520-0469(1989)046<3077:Nsocod>2.0.Co;2
9. Fairall CW, Bradley EF, Hare JE, Grachev AA, Edson JB (2003) Bulk parameterization of air-sea fluxes: Updates and verification for the COARE algorithm. Journal of Climate 16(4):571-591. http://doi.org/10.1175/1520-0442(2003)016<0571:Bpoasf>2.0.Co;2
10. Ge LY, Tao CX, Liang HM (1989) Distributive Features of Heavy Rain on Sub-Synoptic Scale Weather Charts Over the ChiangJiang-HuaiHe River Reaches During the Plum-Rain Seanson. Scientia Meteorologica Sinica 9(01):57-67 (in Chinese)
11. Hsu PC, Li T (2011) Interactions between Boreal Summer Intraseasonal Oscillations and Synoptic-Scale Disturbances over the Western North Pacific. Part II: Apparent Heat and Moisture Sources and Eddy Momentum Transport. Journal of Climate 24(3):942-961. http://doi.org/10.1175/2010jcli3834.1
12. Joseph PV, Sijikumar S (2004) Intraseasonal variability of the low-level jet stream of the Asian summer monsoon. Journal of Climate 17(7):1449-1458. http://doi.org/10.1175/1520-0442(2004)017<1449:Ivotlj>2.0.Co;2
13. Kain JS (2004) The Kain-Fritsch convective parameterization: An update. Journal of Applied Meteorology 43(1):170-181. http://doi.org/10.1175/1520-0450(2004)043<0170:Tkcpau>2.0.Co;2
14. Li L, Zhang RH, Wen M (2011) Diagnostic analysis of the evolution mechanism for a vortex over the Tibetan Plateau in June 2008. Advances in Atmospheric Sciences 28(4):797-808. http://doi.org/10.1007/s00376-010-0027-y
15. Li L, Zhang RH, Wen M, Liu LK (2014) Effect of the atmospheric heat source on the development and eastward movement of the Tibetan Plateau vortices. Tellus Series a-Dynamic Meteorology and Oceanography 66(1):24451. http://doi.org/10.3402/tellusa.v66.24451
16. Li L, Zhang RH, Wen M, Duan JP (2019) Development and eastward movement mechanisms of the Tibetan Plateau vortices moving off the Tibetan Plateau. Climate Dynamics 52(7-8):4849-4859. http://doi.org/10.1007/s00382-018-4420-z

17. Li Y, Chen LS, Wang JZ (2004) The Diagnostic Analysis On The Characteristics Of Large Scale Circulation Corresponding To The Sustaining And Decaying Of Tropical Cyclone After It's Landfall. Acta Meteorologica Sinica 747(2):1112-1112. http://doi.org/10.3321/j.issn:0577-6619.2004.02.004 (in Chinese)
18. Liu BH, Xu M, Henderson M, Qi Y (2005) Observed trends of precipitation amount, frequency, and intensity in China, 1960-2000. Journal of Geophysical Research-Atmospheres 110(D8). http://doi.org/10.1029/2004jd004864
19. Liu YM (1999) The effect of spatially nonuniform heating on the formation and variation of subtropical high Part III : Condensation heating and south Asia high and western Pacific subtropical high. Acta Meteor Sinica 57(5):14. http://doi.org/10.11676/qxxb1999.051 (in Chinese)
20. Luo YL, Wu MW, Ren FM, Li J, Wong WK (2016) Synoptic Situations of Extreme Hourly Precipitation over China. Journal of Climate 29(24):8703-8719. http://doi.org/10.1175/Jcli-D-16-0057.1
21. Mlawer EJ, Taubman SJ, Brown PD, Iacono MJ, Clough SA (1997) Radiative transfer for inhomogeneous atmospheres: RRTM, a validated correlated-k model for the longwave. Journal of Geophysical Research-Atmospheres 102(D14):16663-16682. http://doi.org/10.1029/97jd00237
22. Qian W, Kang HS, Lee DK (2002) Distribution of seasonal rainfall in the East Asian monsoon region. Theoretical and Applied Climatology 73(3-4):151-168. http://doi.org/10.1007/s00704-002-0679-3
23. Ren FM, Cui DL, Gong ZQ, Wang YJ, Zou XK, Li YP, Wang SG, Wang XL (2012) An Objective Identification Technique for Regional Extreme Events. Journal of Climate 25(20):7015-7027. http://doi.org/10.1175/Jcli-D-11-00489.1
24. Sampe T, Xie SP (2010) Large-Scale Dynamics of the Meiyu-Baiu Rainband: Environmental Forcing by the Westerly Jet. Journal of Climate 23(1):113-134. http://doi.org/10.1175/2009jcli3128.1
25. Shao X (2016) East Asian Monsoon Yearbook 2016. Meteorological Press, Beijing
26. Skamarock WC, Klemp JB, Dudhia J, Gill DO, Liu Z, Berner J, Wang W, Powers JG, Duda MG, Barker DM, Huang XY. 2019. A Description of the Advanced Research WRF Version 4. , 145 pp.
27. Tang YB, Gan JJ, Zhao L, Gao K (2006) On the climatology of persistent heavy rainfall events in China. Advances in Atmospheric Sciences 23(5):678-692. http://doi.org/10.1007/s00376-006-0678-x
28. Tao WK, Simpson J, Mccumber M (1989) An Ice Water Saturation Adjustment. Monthly Weather Review 117(1):231-235. http://doi.org/10.1175/1520-0493(1989)117<0231:Aiwsa>2.0.Co;2
29. Tao WK, Wu D, Lang S, Chern JD, Peters-Lidard C, Fridlind A, Matsui T (2016) High-resolution NU-WRF simulations of a deep convective-precipitation system during MC3E: Further improvements and comparisons between Goddard microphysics schemes and observations. J Geophys Res Atmos 121(3):1278-1305. http://doi.org/10.1002/2015JD023986
30. Wang HJ, Sun JH, Wei J, Zhao SX (2014) Classification of Persistent Heavy Rainfall Events over Southern China during Recent 30 Years. Climatic and Environmental Research 19(06):713-725. http://doi.org/10.3878/j.issn.1006-9585.2013.13143 (in Chinese)
31. Wang J (1995) A preliminary analysis of rainstorm and floods in the middle and lower reaches of the Yangtze river from June to July 1995. Urban Bridges and flood control(04):43-49.

http://doi.org/CNKI:SUN:CSDQ.0.1995-04-005 (in Chinese)

32. Wu R, Wang B (2001) Multi-stage onset of the summer monsoon over the western North Pacific. Climate Dynamics 17(4):277-289. http://doi.org/10.1007/s003820000118
33. Wu YJ, Ji HX, Wen JH, Wu SY, Xu M, Tagle F, He B, Duan WL, Li JX (2019) The characteristics of regional heavy precipitation events over eastern monsoon China during 1960-2013. Global and Planetary Change 172(2019):414-427. http://doi.org/10.1016/j.gloplacha.2018.11.001
34. Yanai M, Esbensen S, Chu JH (1973) Determination of Bulk Properties of Tropical Cloud Clusters from Large-Scale Heat and Moisture Budgets. Journal of the Atmospheric Sciences 30(4):611-627. http://doi.org/10.1175/1520-0469(1973)030<0611:Dobpot>2.0.Co;2
35. Ye DZ, Tao SY, Li MC (1958) The Abrupt Change of Circulation over Northern Hemisphere During June and October. Acta Meteor Sinica 29(4):27-41 (in Chinese)
36. Ying M, Zhang W, Yu H, Lu XQ, Feng JX, Fan YX, Zhu YT, Chen DQ (2014) An Overview of the China Meteorological Administration Tropical Cyclone Database. Journal of Atmospheric and Oceanic Technology 31(2):287-301. http://doi.org/10.1175/Jtech-D-12-00119.1
37. Zhang C, Tang QH, Chen DL (2017) Recent Changes in the Moisture Source of Precipitation over the Tibetan Plateau. Journal of Climate 30(5):1807-1819. http://doi.org/10.1175/Jcli-D-15-0842.1
38. Zhang S, Fan BJ (1995) Report of the Damage Caused By Diaster in China 1949-1995. China Statistics Press, Beijing
39. Zhao P, Yang S, Yu RC (2010) Long-Term Changes in Rainfall over Eastern China and Large-Scale Atmospheric Circulation Associated with Recent Global Warming. Journal of Climate 23(6):1544-1562. http://doi.org/10.1175/2009jcli2660.1
40. Zhao W, Chen SF, Chen W, Yao SL, Nath D, Yu B (2019) Interannual variations of the rainy season withdrawal of the monsoon transitional zone in China. Climate Dynamics 53(3-4):2031-2046. http://doi.org/10.1007/s00382-019-04762-9
41. Zhao YF, Zhu J, Xu Y (2014) Establishment and assessment of the grid precipitation datasets in China for recent 50 years Journal of the Meteorological Sciences 34(04):414-420. http://doi.org/10.3969/2013jms.0008 (in Chinese)
42. Zhou YS, Li B (2010) Structural analyses of vortex causing torrential rain over the ChangJiang-Huaihe River basin during 8 and 9 July 2003. Chinese Journal of Atmospheric Sciences 34(3):629-639. http://doi.org/10.3878/j.issn.1006-9895.2010.03.14 (in Chinese)
43. Zou XK, Ren FM (2015) Changes in Regional Heavy Rainfall Events in China during 1961-2012. Advances in Atmospheric Sciences 32(5):704-714. http://doi.org/10.1007/s00376-014-4127-y

Figures

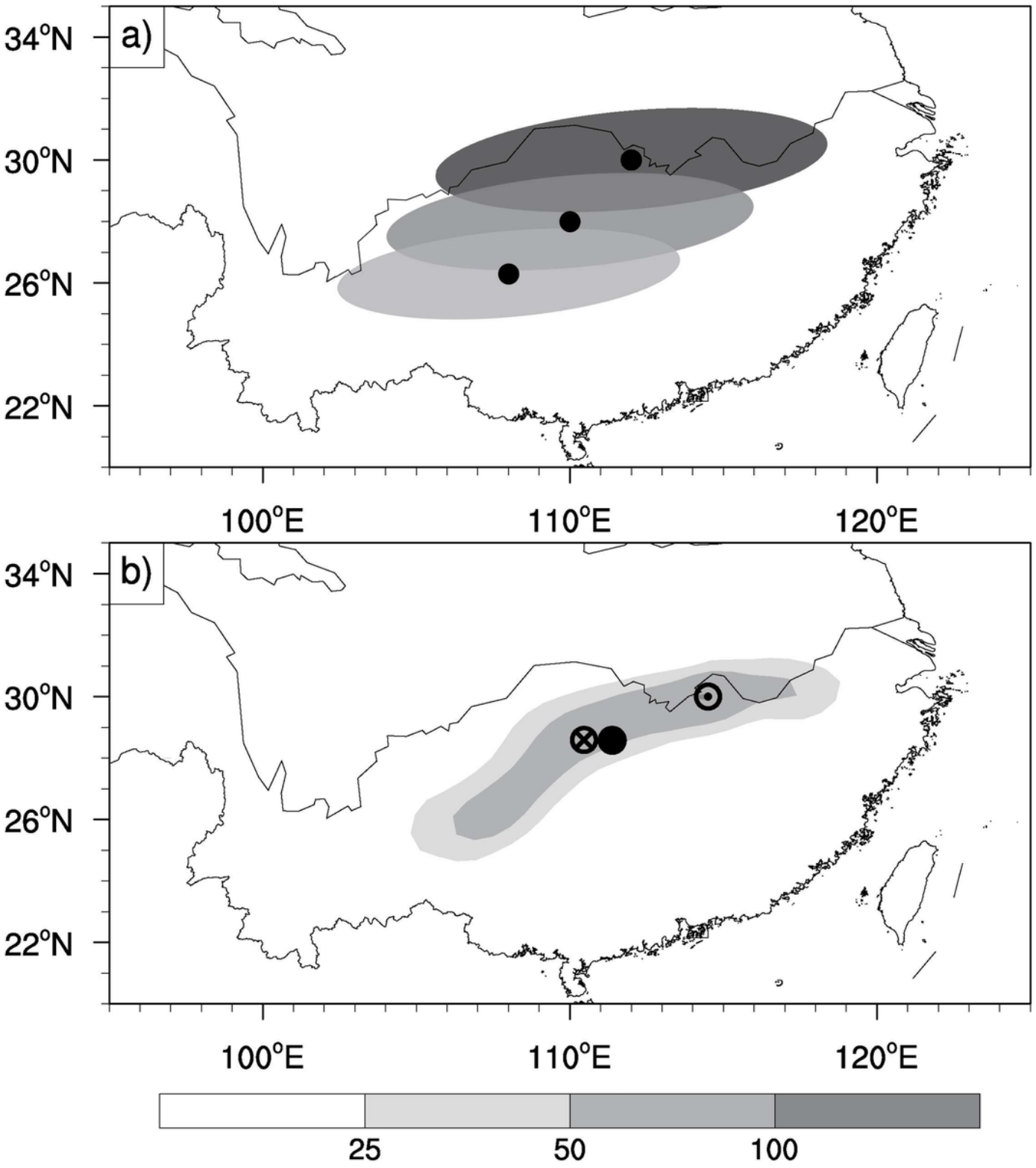

Figure 1

(a) The schematic illustration of the technique used to identify an LPEPE (a) The deep gray, moderate gray, and light gray are the LEP on the first, second and third day. (b) the precipitation (shadings, unit: mm) and the central location of LEP using three different methods: MP (dot in a circle), WP (the black dot), and AP (cross in circle) of an LPEPE randomly chosen on Jun 21st, 1986

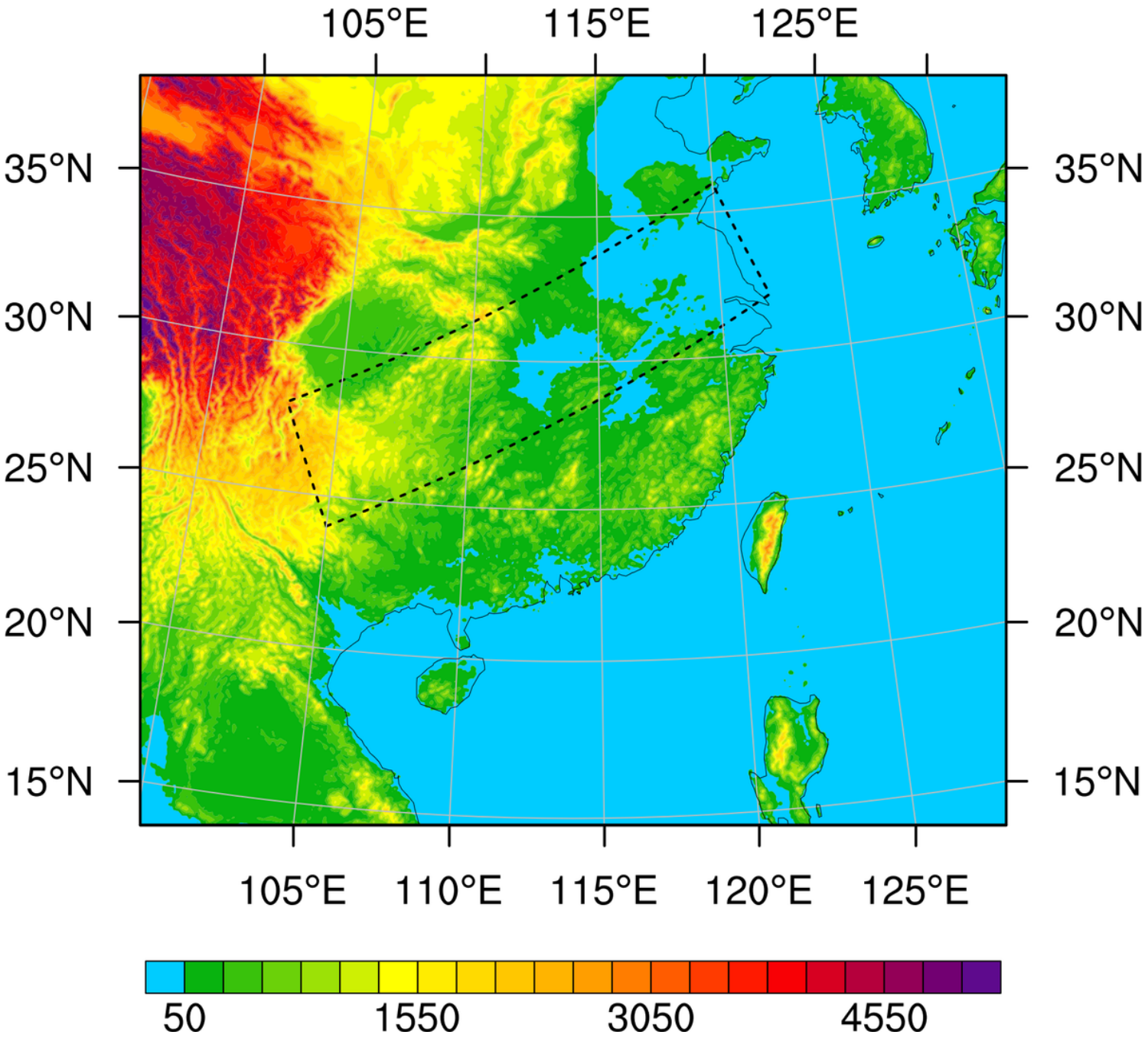

Figure 2

The terrain height of the simulation area. The grid resolution is 5km, and the grid number is 652×565. The dashed box is the concerned area of LPEPE from 8th to 10th July 2003.

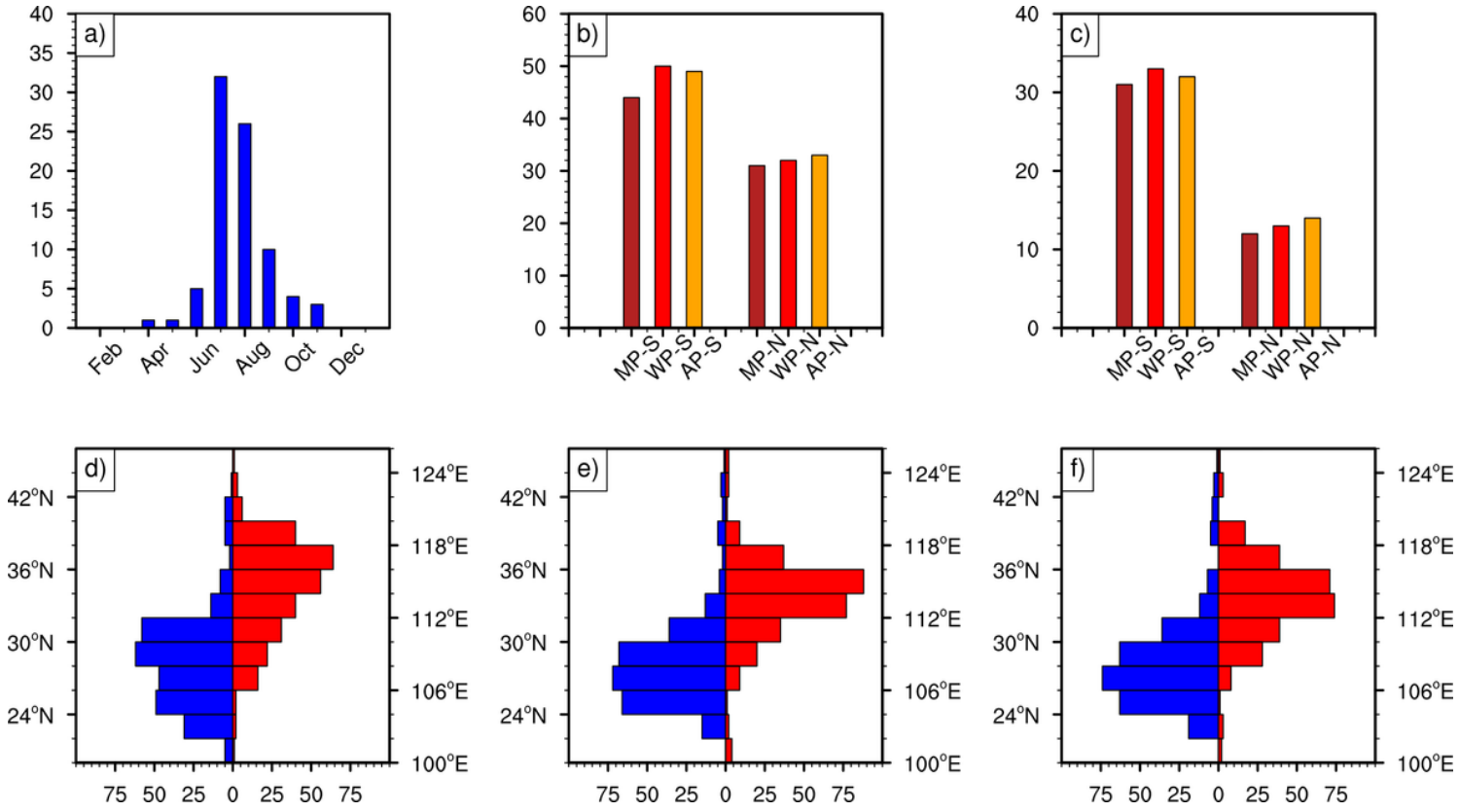

Figure 3

(a) The monthly distribution of all LPEPEs, (b) moving direction distribution of all LPEPEs, (c) moving direction distribution of all LPEPEs during Mei-yu period, and the meridional and zonal distribution of all LEPs using (d) MPs, (e) WPs, and (f) APs. The moving direction is determined by the latitude change of MPs, WPs and APs between the first day and last day of the LPEPEs. “S” is for the southward-moving LPEPEs; “N” is for the northward-moving LPEPEs.

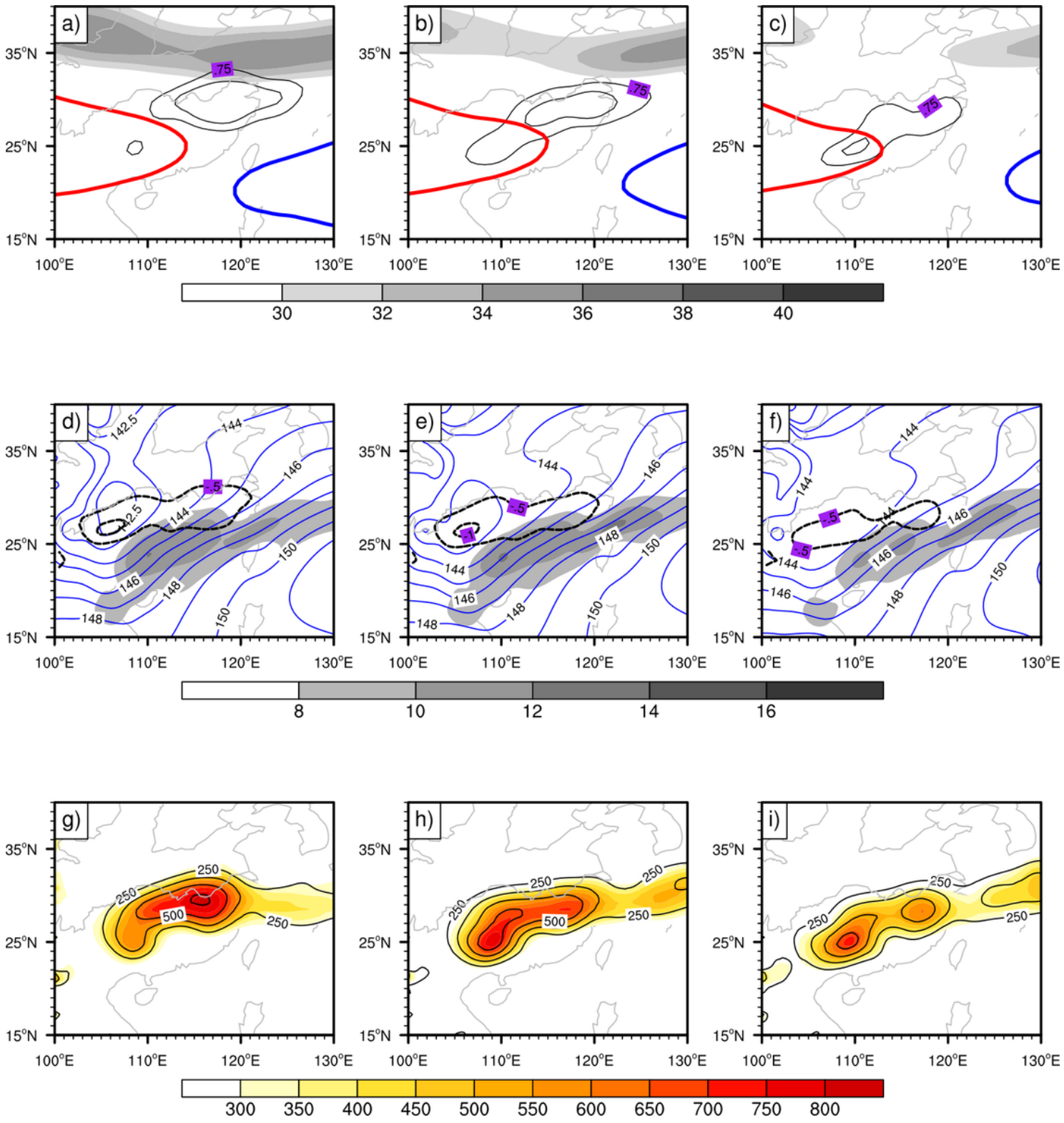

Figure 4

The composite circulation analysis of dynamical and thermodynamical characters of 33 southward-moving LPEPEs-M from the first to the third day. (a-c) the high-level jet (200 hPa, shades, units: m s^{-1}), the divergence region at 200hPa (black contours, units: $\times 10^{-5} \cdot s^{-1}$), the WPSH (588 dagpm at 500hPa, blue contours) and the SAH (1252 dagpm at 200hPa, red contours) from the first to the third day. (d-f) the low-level jet (850 hPa, shades, units: $kg \cdot kg^{-1}$), the geopotential height at 850 hPa (blue contour, units: dagpm),

and the convergence region (dash contours, units: $\times 10^{-5} \cdot s^{-1}$) at 850hPa. (g-i) is the vertical integral of *Q1* (shades, units: $W \cdot s^{-1}$)) and *Q2* (contour, units: $W \cdot s^{-1}$).

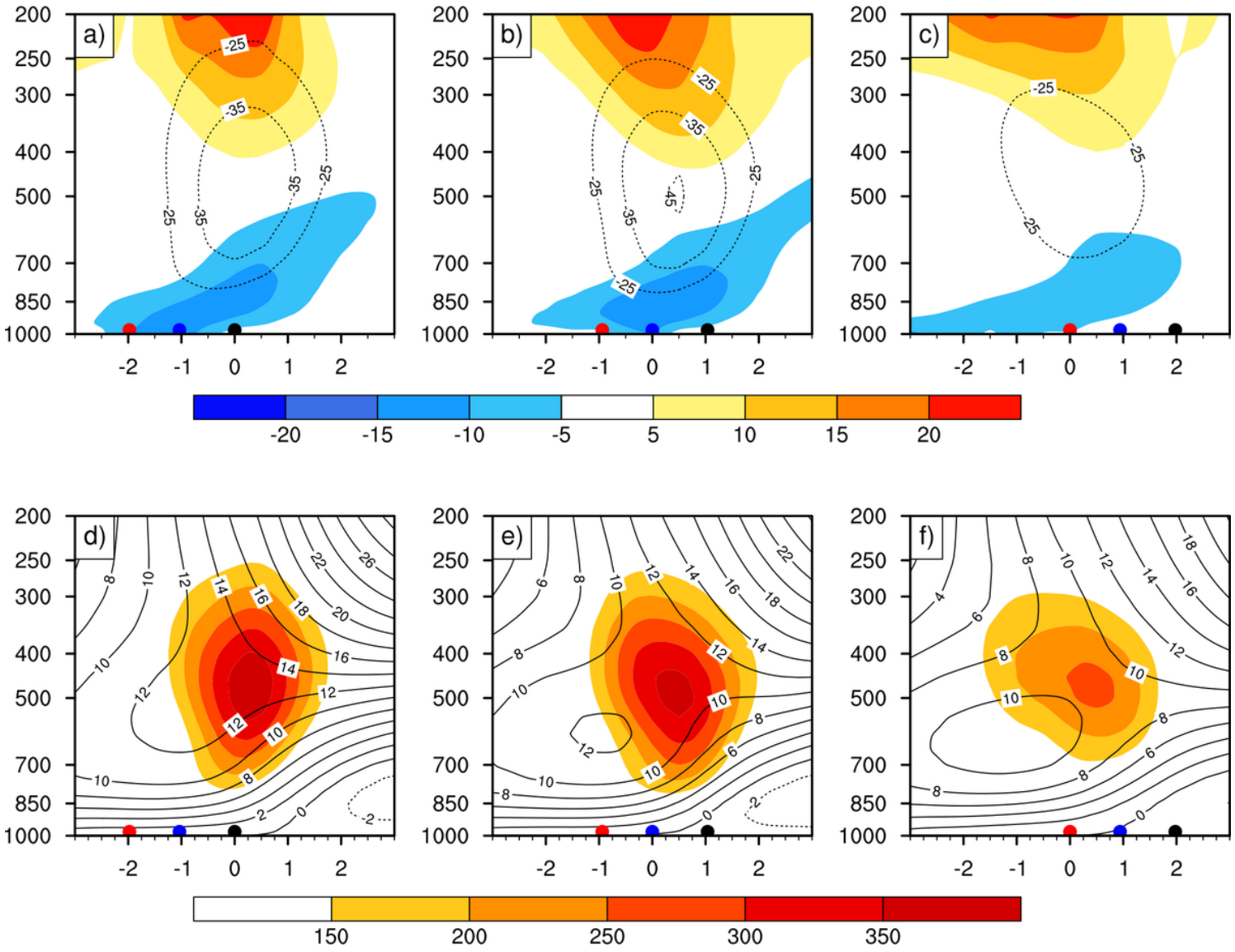

Figure 5

The dynamic composite analysis of vertical cross-section along the Lon_{wp} from the first day to the third day. (a–c) the convergence (shades, units: $\times 10^{-6} \cdot s^{-1}$) and vertical velocity (dash lines, units: $\times 10^{-2} \cdot pa \cdot s^{-1}$). (d-f) the Q_1 (shades, units: $\times 10^{-6} \cdot K \cdot s^{-1}$ and zonal wind (contour, units: $m \cdot s^{-1}$). The black, blue, and red dot is dynamic composite Lat_{wp} on the first, second and third day of LPEPEs.

Figure 6

The dynamic composite analysis of *PE1* (a-c), *PE2* (d-f), *PE3* (g-i), *PE4* (j-l), *PE5* (m-o), *PE6* (p-r) (shades, units: PVU, 1PVU=$\times 10^{-12}$ $m^2 \cdot s^{-2} \cdot K \cdot Kg^{-1}$) at 850hPa and the dynamic composite rainband (lines, 50mm).

The X-axis is the longitude departure (units: degree) from the WPs (0,0), The Y-axis is the latitude departure (units: degree) from the WPs (0,0).

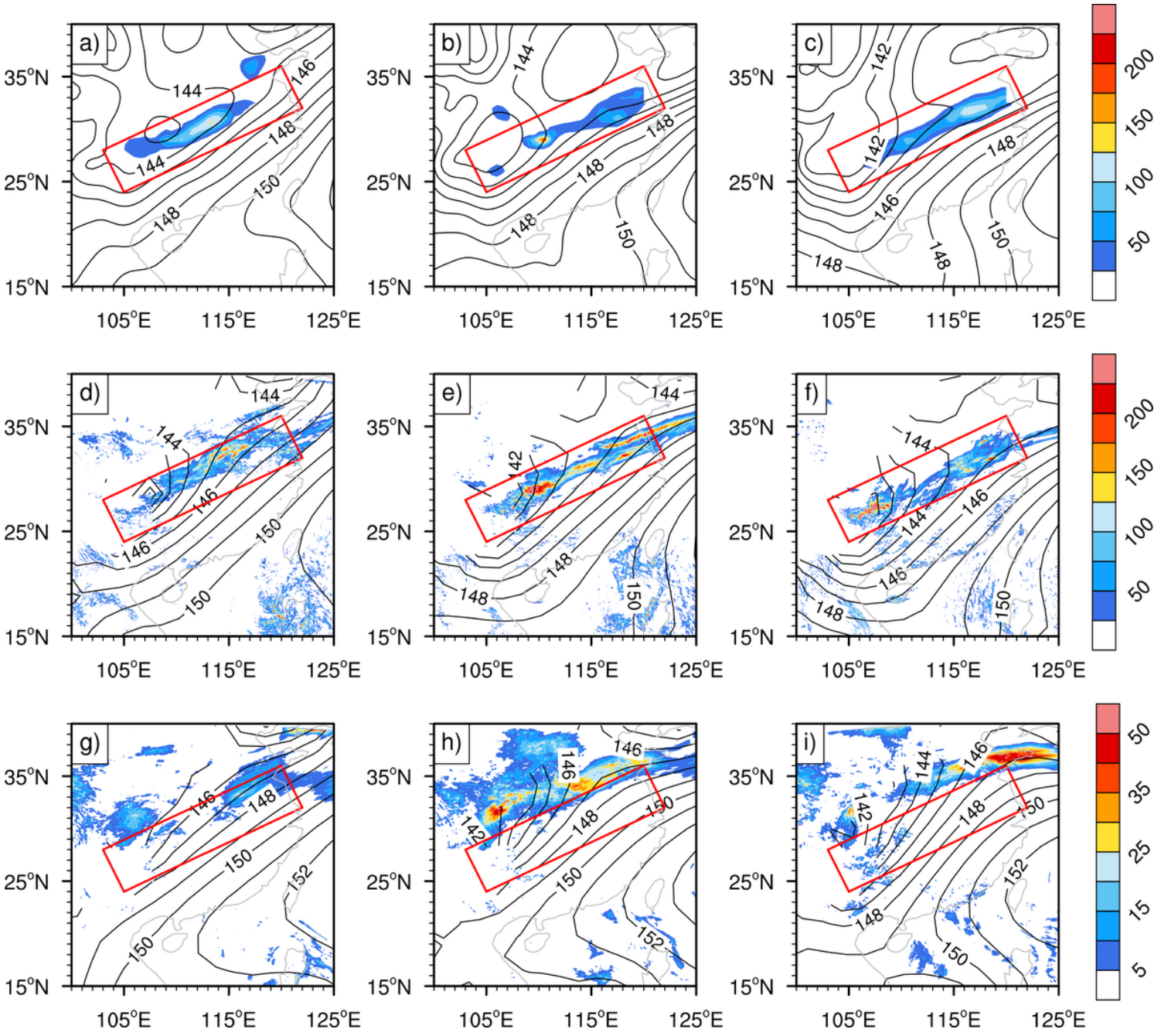

Figure 7

The daily precipitation (shades, units: mm/day) and the geopotential height (contour, units: dagpm) at 850hPa for observation (a–c), control run (d-f), and sensitivity run (g-i). The red boxes are the concerned area of the LPEPE on 8th to 10th July, 2003.

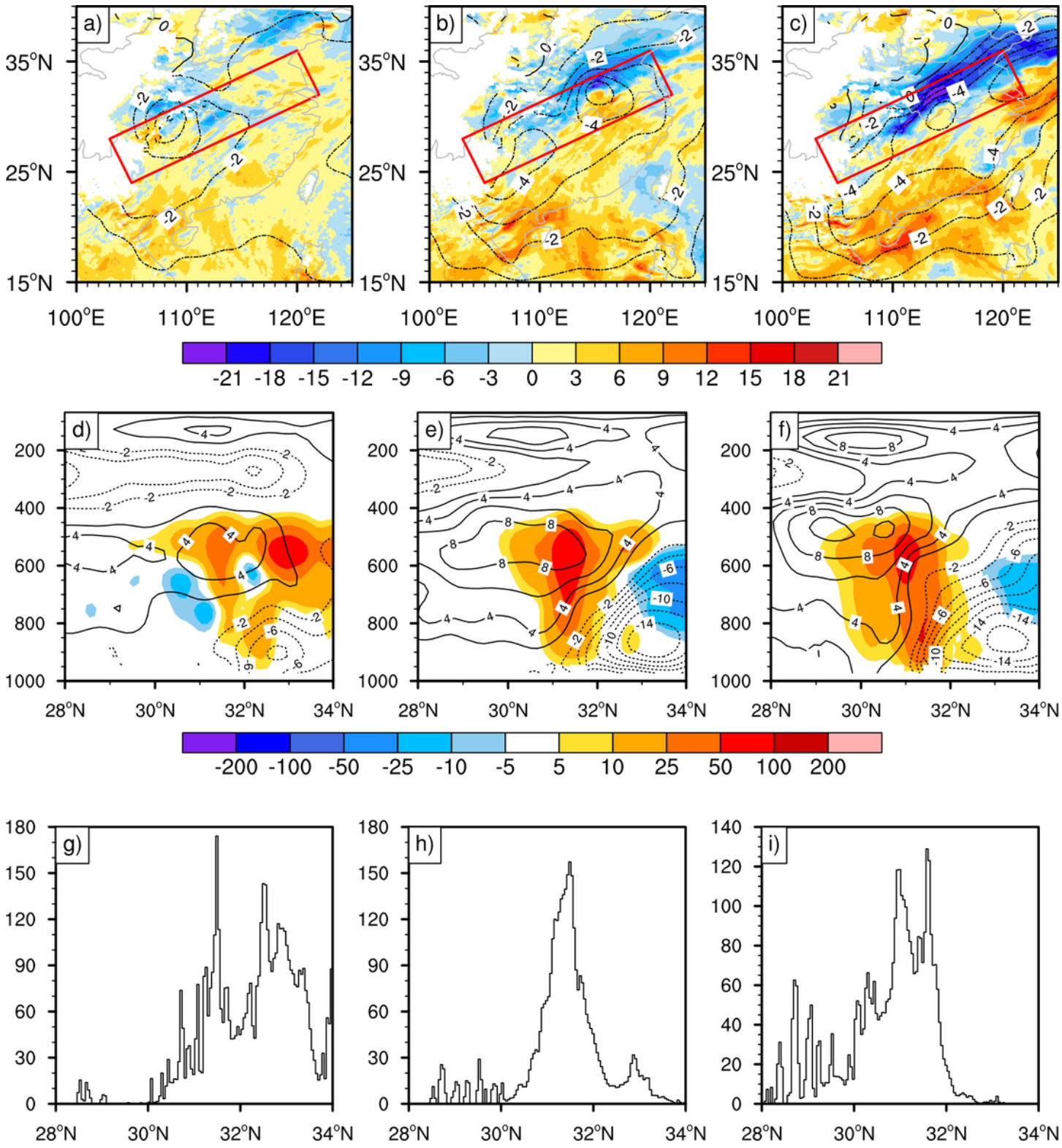

Figure 8

(a-c) the zonal wind difference (shades, units: m) and the geopotential height difference (contours, units: dagpm) between control and sensitivity runs. (d-f) the daily condensation latent heat difference (shades, units: K) and the daily averaged meridional wind difference (contour, units: $m \cdot s^{-1}$) between control and sensitivity runs along the 115°E vertical cross-section. (g-i) the daily precipitation in CTRL along 115°E (units: mm).